

*Journal of*  
***Mechanics of***  
***Materials and Structures***

**CYCLIC BEHAVIOR AND ENERGY APPROACH TO THE FATIGUE  
OF SHAPE MEMORY ALLOYS**

Ziad Moumni, Wael Zaki and Habibou Maitournam

***Volume 4, N° 2***

***February 2009***



## CYCLIC BEHAVIOR AND ENERGY APPROACH TO THE FATIGUE OF SHAPE MEMORY ALLOYS

ZIAD MOUMNI, WAEL ZAKI AND HABIBOU MAITOURNAM

We present an energy-based low-cycle fatigue criterion that can be used in analyzing and designing structures made from shape memory alloys subjected to cyclic loading. Experimentally, a response similar to plastic shakedown is observed. During the first cycles the stress-strain curve shows a hysteresis loop which evolves during the first few cycles before stabilizing. By adopting an analogy with plastic fatigue, it is shown that the dissipated energy of the stabilized cycle is a relevant parameter for estimating the number of cycles to failure of such materials. Following these observations, we provide an application of the cyclic model, previously developed by the authors within the framework of generalized standard materials with internal constraints in order to evaluate such parameter. Numerical simulations are presented along with a validation against experimental data in case of cyclic superelasticity.

### 1. Introduction

The interesting behavior of SMAs (shape memory alloys) is essentially due to their capability of undergoing a reversible diffusionless solid–solid phase transition known as the martensitic transformation [Wayman and Otsuka 1999; Shaw and Kyriakides 1995; Moumni et al. 2008]. This transition is characterized at the microscopic level by a modification of the crystallographic lattice structure which can be induced by altering either the material temperature or the stress to which it is subjected or both, hence a strong thermomechanical coupling. At high temperatures, a shape memory alloy consists of a relatively ordered parent phase called austenite which transforms when cooled into a less ordered product phase called martensite. In the absence of stress, this leads to self-accommodation of martensite plates, that is, to the formation of lattice twins without any macroscopic deformation.

Mechanical loading may lead to detwinning of self-accommodating martensite. In this case, martensite plates become oriented according to privileged directions that depend on the applied stress. The resulting inelastic macroscopic strain usually reaches several percent; it can be recovered by heating, in which case the SMA regains its initial undeformed austenitic shape. Simple way shape memory refers to the ability of a shape memory alloy to remember its high temperature state.

Besides the characteristic shape memory behavior, SMAs exhibit other interesting effects, namely: superelasticity or pseudoelasticity, which is the ability of a shape memory alloy to accommodate large strains due to stress-induced phase change at a constant and sufficiently high temperature and to recover its undeformed shape upon unloading; and the superthermal effect, which is the ability to deform an initially austenitic SMA by cooling under constant stress and then to recover the austenitic shape by heating. The magnitude of the temperature-induced strains depends on the applied stress.

---

*Keywords:* cyclic pseudoelasticity, shape memory alloys, SMA fatigue, cyclic loading, residual strain, internal stress, dissipation.

Furthermore, cyclic loading may allow SMAs to have a two-way shape memory effect. In this case, the material can change its shape reversibly due to cyclic heating-cooling.

Since components made of SMAs usually operate under cyclic thermomechanical loading; their design requires reliable prediction of the material's cyclic three-dimensional response and fatigue resistance. In this regard, several models exist that are capable of handling cyclic, mainly superelastic, SMA behavior; see, for instance, [Liu et al. 1999; Abeyaratne and Kim 1997; Lim and McDowell 2002; Tanaka et al. 1995; Lexcellent and Bourbon 1996; Bo and Lagoudas 1999; Zaki and Moumni 2007a].

The interesting properties of SMAs promoted their use in several fields, especially in outer space (antennas, braces) and in medical applications (orthodontia, cardiology, implant miniaturization, etc.). SMAs are also becoming increasingly attractive for automotive, nuclear, and civil engineering applications, mainly due to their high damping capacity.

One of the main difficulties facing their use in technologically advanced applications with high safety specifications is the poorly known fatigue behavior of these alloys; another is the amnesia phenomenon. Better knowledge and control of these two aspects should promote their use. Two types of fatigue have to be considered.

First, classical mechanical fatigue due to mechanical cycling in the pseudoelastic domain [Miyazaki et al. 1986; Van Humbeeck 1991]. The objective is to determine the number of cycles before failure. For instance, SMAs are used in the biomedical field to manufacture stents, endovascular prostheses inserted in blood vessels to avoid thrombosis and occlusion of the vessels. In stents, cyclic loads would arise from the difference in systolic and diastolic blood pressures and from the stress associated with the contraction of the heart muscle [McKelvey and Ritchie 1999]. It is of primary importance to know the number of cycles before any damage occurs to the stent.

Second, thermal fatigue or amnesia of the material due to a degradation of the material characteristics responsible for the shape memory effect like the transformation temperatures. The question is to determine if the material remains able to remember its initial shape.

Fatigue of shape memory alloys has also attracted considerable attention [Melton and Mercier 1979a; 1979b; 1979c; Wagner et al. 2004; Vaidyanathan et al. 2000; Porter et al. 2001]; it is still, however, not very well understood. In particular, fatigue mechanisms at the microscopic level are still being investigated [Siredey et al. 2005; Predki et al. 2006]. Nevertheless, Manson–Coffing-type criteria have been successfully used for predicting fatigue induced failure of simple SMA structures subjected to uniaxial loading [Melton and Mercier 1979a; Siredey et al. 2005; Wagner et al. 2004]. Like in classical elastoplastic materials, such as steel, the number of cycles to failure of a SMA varies depending on its composition and on the applied loading, among other factors. This number may range from  $10^4$  cycles for thermal valves using one-way shape memory effect [Eggeler et al. 2004] to a nominal  $4 \times 10^8$  cycles for stents [Morgan 2004].

Using the analogy with plastic fatigue (low-cycle fatigue) [Halford 1966; Charkaluk et al. 2002], a relation was established in [Moumni et al. 2005] between the amount of dissipated energy associated with the stabilized hysteresis cycle and the number of cycles to failure. In this paper, we provide an application of the cyclic model, developed previously by the authors within the framework of generalized standards materials with internal constraints [Moumni et al. 2008], in order to simulate the dissipated energy at the stabilized cycle. Our aim here is to show that the cyclic model can be combined with the fatigue criterion in order to predict low-cycle failure of superelastic shape memory structures.

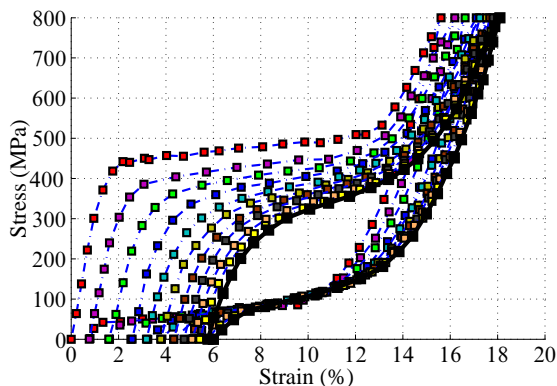


**Figure 1.** Cyclic superelastic tensile response of a NiTi wire. The characteristic hysteresis loop tends to stabilize when the number of cycles increases.

Section 2 is devoted to the presentation of the cyclic Zaki–Moumni model, where the behavior is described using three state variables representing residual strain induced by cyclic loading, internal stress induced by repeated phase change, and the cumulated martensite volume fraction. See [Zaki and Moumni 2007a; 2007b] for a detailed discussion of the model. Section 3 discusses the low cycle fatigue law and numerical simulations of the dissipated energy at the stabilized cycle, along with a validation against experimental data in the case of cyclic superelasticity.

## 2. The cyclic model of SMA behavior

**2.1. Experimental observations.** The response of a nickel-titanium wire to repeated tension, illustrated in Figure 1, displays the following features:

- Recovery of inelastic strain is not complete at the end of each cycle; after complete unloading, some residual strain remains. This strain increases exponentially with the number of cycles, as shown in Figure 2, left.
- Forward phase change yield stress decreases with increasing number of cycles (Figure 2, right).

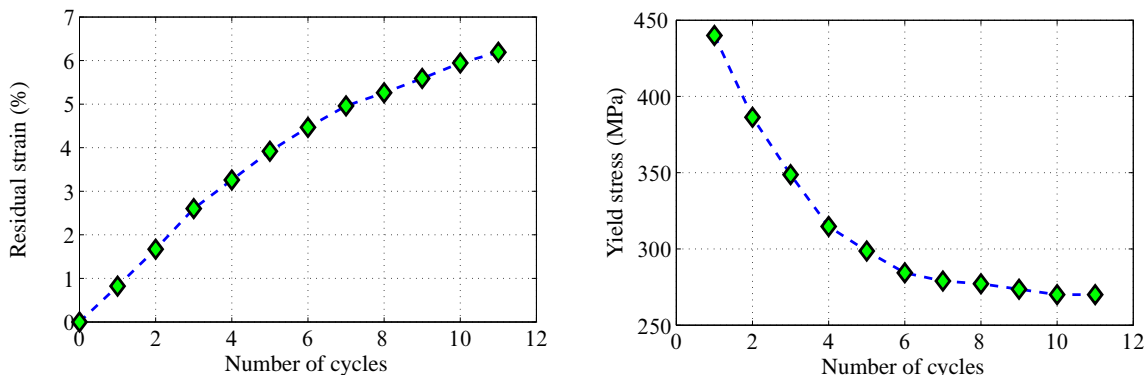


**Figure 2.** Left: residual strain versus number of tensile loading cycles. Right: forward phase change yield stress versus number of cycles.

- The hysteresis loop evolves progressively with the number of cycles before stabilizing. In Figure 1, the stabilized loop is shown by a continuous dark line.

Residual strain is generally considered to be due to some oriented martensite not transforming back into austenite during reverse phase change [Lexcelent and Bourbon 1996; Auricchio et al. 2003]. Repeated forward and reverse phase changes create some defects within the material [Abeyaratne and Kim 1997], which result in localized internal stresses [Tanaka et al. 1995], allowing SMAs to exhibit two-way shape memory. In this case the material is said to be trained (training phenomena). The internal stress eliminates the need for external loading in order to orient martensite variants. As a result, the shape memory structure can assume two different shapes when the temperature varies: an austenitic undeformed shape at high temperatures and a deformed low-temperature shape resulting from martensite orientation due to internal stress.

**2.2. Phenomenological model.** For full details regarding the model presented in this section, the reader is referred to [Zaki 2006; Zaki and Moumni 2007a; 2007b; Moumni et al. 2008].

As seen in the previous section, the macroscopic cyclic response of superelastic SMAs induces residual inelastic strains and localized internal stresses within the material. Hence, two state variables are introduced: a residual strain tensor  $\boldsymbol{\epsilon}_r$  and an internal stress tensor  $\mathbf{B}$ . A third variable  $z_e$  representing cumulated martensite volume fraction is also used:

$$z_e = \int_0^t |\dot{z}| d\tau,$$

where  $t$  is a kinematic time. The effect of cyclic loading on the material parameters can be modeled by considering these parameters to depend on  $z_e$ .

**2.2.1. State variables and free energy.** The following state variables are considered

- Macroscopic strain  $\boldsymbol{\epsilon}$  and temperature  $T$ .
- Volume fraction  $z$  and cumulated volume fraction  $z_e$  of martensite.
- Local strain tensors:  $\boldsymbol{\epsilon}_A$  for austenite and  $\boldsymbol{\epsilon}_M$  for martensite.
- Local martensite transformation strain tensor  $\boldsymbol{\epsilon}_{tr}$ .
- Internal stress  $\mathbf{B}$  and residual strain  $\boldsymbol{\epsilon}_r$ .

Phase change latent heat is assumed to depend on the cumulated fraction  $z_e$ . The respective free energy densities of austenite and martensite are taken to be

$$\mathcal{W}_A \stackrel{\text{def}}{=} W_A(\boldsymbol{\epsilon}_A, \boldsymbol{\epsilon}_r) = \frac{1}{2}(\boldsymbol{\epsilon}_A - \boldsymbol{\epsilon}_r) : \mathbf{K}_A : (\boldsymbol{\epsilon}_A - \boldsymbol{\epsilon}_r),$$

and

$$\mathcal{W}_M = W_M(\boldsymbol{\epsilon}_M, \boldsymbol{\epsilon}_{tr}, \boldsymbol{\epsilon}_r, T, \mathbf{B}, z_e) = \frac{1}{2}(\boldsymbol{\epsilon}_M - \boldsymbol{\epsilon}_{tr} - \boldsymbol{\epsilon}_r) : \mathbf{K}_M : (\boldsymbol{\epsilon}_M - \boldsymbol{\epsilon}_{tr} - \boldsymbol{\epsilon}_r) + C(T, z_e) - \frac{2}{3}\mathbf{B} : \boldsymbol{\epsilon}_{tr}.$$

$\mathbf{B} : \boldsymbol{\epsilon}_{tr}$  in the expression of  $\mathcal{W}_M$  allows modeling the two-way shape memory effect. It represents a modification of the free energy of martensite due to the creation of internal stresses, which allows austenite to transform more easily into oriented martensite. Subsequent sections will help clarify this idea, especially when phase change criteria are established.

The contribution of austenite–martensite interaction to the SMA free energy density is assumed to be

$$\mathcal{F} = I(z, z_e, \boldsymbol{\varepsilon}_{tr}) = G \frac{z^2}{2} + \frac{z}{2} [\alpha z + \beta(1-z)] \left( \frac{2}{3} \boldsymbol{\varepsilon}_{tr} : \boldsymbol{\varepsilon}_{tr} \right).$$

$G$ ,  $\alpha$  and  $\beta$  are material parameters functions of the cumulated martensite volume fraction  $z_e$  ( $G = \hat{G}(z_e)$ ,  $\alpha = \hat{\alpha}(z_e)$ , and  $\beta = \hat{\beta}(z_e)$ )

- $\beta \frac{z(1-z)}{2} \left( \frac{2}{3} \boldsymbol{\varepsilon}_{tr} : \boldsymbol{\varepsilon}_{tr} \right)$  represents interaction between austenite and martensite. Following many published works [Leclercq and Lexcellent 1996; Raniecki et al. 1992; Patoor and Berveiller 1993, etc.], this interaction is taken to be proportional to the volume fractions of interacting phases.  $\beta$  determines how a mechanical loading applied to an initially austenitic shape memory material affects martensite orientation during phase change.
- $G \frac{z^2}{2}$  quantifies orientation-independent interaction between martensite variants.
- $\alpha \frac{z^2}{2} \left( \frac{2}{3} \boldsymbol{\varepsilon}_{tr} : \boldsymbol{\varepsilon}_{tr} \right)$  accounts for the interaction increase due to orientation of martensite plates; its expression is similar to that of the energy contribution due to linear kinematic hardening of an elastoplastic material with hardening coefficient  $\alpha$ .  $\alpha$  controls the slope of the stress-strain curve corresponding to martensite orientation.

Finally, the free energy density of the material is given by

$$\begin{aligned} \mathcal{W} &\stackrel{\text{def}}{=} W(\boldsymbol{\varepsilon}, T, \boldsymbol{\varepsilon}_A, \boldsymbol{\varepsilon}_M, z, \boldsymbol{\varepsilon}_{tr}, \boldsymbol{\varepsilon}_r, \mathbf{B}, z_e) \\ &= (1-z) \left[ \frac{1}{2} (\boldsymbol{\varepsilon}_A - \boldsymbol{\varepsilon}_r) : \mathbf{K}_A : \boldsymbol{\varepsilon}_A - \boldsymbol{\varepsilon}_r \right] + z \left[ \frac{1}{2} (\boldsymbol{\varepsilon}_M - \boldsymbol{\varepsilon}_{tr} - \boldsymbol{\varepsilon}_r) : \mathbf{K}_M : (\boldsymbol{\varepsilon}_M - \boldsymbol{\varepsilon}_{tr} - \boldsymbol{\varepsilon}_r) + C(T, z_e) \right] \\ &\quad + \frac{1}{2} G z^2 + \frac{1}{2} z [\alpha z + \beta(1-z)] \left( \frac{2}{3} \boldsymbol{\varepsilon}_{tr} : \boldsymbol{\varepsilon}_{tr} \right) - \frac{2}{3} z \mathbf{B} : \boldsymbol{\varepsilon}_{tr}. \quad (1) \end{aligned}$$

**2.2.2. Internal constraints and Lagrangian.** State variables obey the following constraints

- Martensite volume fraction is necessarily within the  $[0, 1]$  interval.

$$z \geq 0, \quad (1-z) \geq 0. \quad (2)$$

- The equivalent transformation strain  $\sqrt{\frac{2}{3} \boldsymbol{\varepsilon}_{tr} : \boldsymbol{\varepsilon}_{tr}}$  has a maximum value  $\gamma$  that varies with respect to the cumulated volume fraction  $z_e$

$$\gamma - \sqrt{\frac{2}{3} \boldsymbol{\varepsilon}_{tr} : \boldsymbol{\varepsilon}_{tr}} \geq 0, \quad \gamma \stackrel{\text{def}}{=} \hat{\gamma}(z_e). \quad (3)$$

Constraints given by (2) and (3) are assumed to be perfect. They derive from a constraints potential

$$\mathcal{W}_l = -\lambda : [(1-z)\boldsymbol{\varepsilon}_A + z\boldsymbol{\varepsilon}_M - \boldsymbol{\varepsilon}] - \mu \left( \gamma - \sqrt{\frac{2}{3} \boldsymbol{\varepsilon}_{tr} : \boldsymbol{\varepsilon}_{tr}} \right) - \nu_1 z - \nu_2 (1-z),$$

where  $\lambda$ ,  $\nu_1$ ,  $\nu_2$ , and  $\mu$  are Lagrange multipliers.  $\nu_1$ ,  $\nu_2$  and  $\mu$ , associated with unilateral constraints, must obey the following conditions

$$\nu_1 \geq 0, \nu_1 z = 0, \quad \nu_2 \geq 0, \nu_2 (1-z) = 0 \quad \text{and} \quad \mu \geq 0, \mu \left( \gamma - \sqrt{\frac{2}{3} \boldsymbol{\varepsilon}_{tr} : \boldsymbol{\varepsilon}_{tr}} \right) = 0. \quad (4)$$

The sum of the free energy  $\mathcal{W}$  and of the constraints potential  $\mathcal{W}_l$  gives the Lagrangian

$$\begin{aligned} \mathcal{L} &= \mathcal{W} + \mathcal{W}_l \stackrel{\text{def}}{=} L(\boldsymbol{\varepsilon}, T, \boldsymbol{\varepsilon}_A, \boldsymbol{\varepsilon}_M, z, \boldsymbol{\varepsilon}_{\text{tr}}, \boldsymbol{\varepsilon}_r, \mathbf{B}, z_e) \\ &= (1-z) \left[ \frac{1}{2} (\boldsymbol{\varepsilon}_A - \boldsymbol{\varepsilon}_r) : \mathbf{K}_A : (\boldsymbol{\varepsilon}_A - \boldsymbol{\varepsilon}_r) \right] + z \left[ \frac{1}{2} (\boldsymbol{\varepsilon}_M - \boldsymbol{\varepsilon}_{\text{tr}} - \boldsymbol{\varepsilon}_r) : \mathbf{K}_M : (\boldsymbol{\varepsilon}_M - \boldsymbol{\varepsilon}_{\text{tr}} - \boldsymbol{\varepsilon}_r) + C(T, z_e) - \frac{2}{3} \mathbf{B} : \boldsymbol{\varepsilon}_{\text{tr}} \right] \\ &\quad + G \frac{1}{2} z^2 + \frac{1}{2} z [\alpha z + \beta(1-z)] \left( \frac{2}{3} \boldsymbol{\varepsilon}_{\text{tr}} : \boldsymbol{\varepsilon}_{\text{tr}} \right) \\ &\quad - \boldsymbol{\lambda} : [(1-z)\boldsymbol{\varepsilon}_1 + z\boldsymbol{\varepsilon}_2 - \boldsymbol{\varepsilon}] - \mu \left( \gamma - \sqrt{\frac{2}{3} \boldsymbol{\varepsilon}_{\text{tr}} : \boldsymbol{\varepsilon}_{\text{tr}}} \right) - \nu_1 z - \nu_2 (1-z), \end{aligned} \quad (5)$$

where conditions (4) must be met.

**2.2.3. State equations.** Phase change, martensite orientation, training, as well as the creation of residual strain and internal stress are dissipative processes. Thus, if  $\mathcal{A}_z$ ,  $\mathcal{A}_{\text{tr}}$ ,  $\mathcal{A}_e$ ,  $\mathcal{A}_r$ , and  $\mathcal{A}_B$  represent thermodynamic forces associated with state variables  $z$ ,  $\boldsymbol{\varepsilon}_{\text{tr}}$ ,  $z_e$ ,  $\boldsymbol{\varepsilon}_r$ , and  $\mathbf{B}$  respectively; only these forces may take nonzero values during a given transformation. Hence the state equations

$$\frac{\partial \mathcal{L}}{\partial \boldsymbol{\varepsilon}} = \boldsymbol{\sigma} \quad \Rightarrow \quad \boldsymbol{\lambda} - \boldsymbol{\sigma} = \mathbf{0}, \quad (6)$$

$$-\frac{\partial \mathcal{L}}{\partial \boldsymbol{\varepsilon}_A} = \mathbf{0} \quad \Rightarrow \quad (1-z) [\mathbf{K}_A : (\boldsymbol{\varepsilon}_A - \boldsymbol{\varepsilon}_r) - \boldsymbol{\lambda}] = \mathbf{0}, \quad (7)$$

$$-\frac{\partial \mathcal{L}}{\partial \boldsymbol{\varepsilon}_M} = \mathbf{0} \quad \Rightarrow \quad z [\mathbf{K}_M : (\boldsymbol{\varepsilon}_M - \boldsymbol{\varepsilon}_{\text{tr}} - \boldsymbol{\varepsilon}_r) - \boldsymbol{\lambda}] = \mathbf{0}, \quad (8)$$

$$\begin{aligned} -\frac{\partial \mathcal{L}}{\partial z} = \mathcal{A}_z \quad \Rightarrow \quad \mathcal{A}_z &= \frac{1}{2} [(\boldsymbol{\varepsilon}_A - \boldsymbol{\varepsilon}_r) : \mathbf{K}_A : (\boldsymbol{\varepsilon}_A - \boldsymbol{\varepsilon}_r) - (\boldsymbol{\varepsilon}_M - \boldsymbol{\varepsilon}_{\text{tr}} - \boldsymbol{\varepsilon}_r) : \mathbf{K}_M : (\boldsymbol{\varepsilon}_M - \boldsymbol{\varepsilon}_{\text{tr}} - \boldsymbol{\varepsilon}_r)] \\ &\quad - C(T, z_e) - Gz - [(\alpha - \beta)z + \frac{1}{2}\beta] \left( \frac{2}{3} \boldsymbol{\varepsilon}_{\text{tr}} : \boldsymbol{\varepsilon}_{\text{tr}} \right) - \boldsymbol{\lambda} : (\boldsymbol{\varepsilon}_A - \boldsymbol{\varepsilon}_M) + \frac{2}{3} \mathbf{B} : \boldsymbol{\varepsilon}_{\text{tr}}, \end{aligned}$$

$$-\frac{\partial \mathcal{L}}{\partial \boldsymbol{\varepsilon}_{\text{tr}}} = \mathcal{A}_{\text{tr}} \quad \Rightarrow \quad \mathcal{A}_{\text{tr}} = z [\mathbf{K}_M : (\boldsymbol{\varepsilon}_M - \boldsymbol{\varepsilon}_{\text{tr}} - \boldsymbol{\varepsilon}_r) - \frac{2}{3} [\alpha z + \beta(1-z)] \boldsymbol{\varepsilon}_{\text{tr}}] + \frac{2}{3} z \mathbf{B} - \frac{2}{3} \mu \boldsymbol{\varepsilon}_{\text{tr}} / \sqrt{\frac{2}{3} \boldsymbol{\varepsilon}_{\text{tr}} : \boldsymbol{\varepsilon}_{\text{tr}}},$$

$$-\frac{\partial \mathcal{L}}{\partial \boldsymbol{\lambda}} = \mathbf{0} \quad \Rightarrow \quad (1-z)\boldsymbol{\varepsilon}_A + z\boldsymbol{\varepsilon}_M - \boldsymbol{\varepsilon} = \mathbf{0}, \quad (9)$$

$$-\frac{\partial \mathcal{L}}{\partial \boldsymbol{\varepsilon}_r} = \mathcal{A}_r \quad \Rightarrow \quad \mathcal{A}_r = (1-z)\mathbf{K}_A : (\boldsymbol{\varepsilon}_A - \boldsymbol{\varepsilon}_r) + z\mathbf{K}_M : (\boldsymbol{\varepsilon}_M - \boldsymbol{\varepsilon}_{\text{tr}} - \boldsymbol{\varepsilon}_r),$$

$$-\frac{\partial \mathcal{L}}{\partial \mathbf{B}} = \mathcal{A}_B \quad \Rightarrow \quad \mathcal{A}_B = \frac{2}{3} z \boldsymbol{\varepsilon}_{\text{tr}},$$

$$-\frac{\partial \mathcal{L}}{\partial z_e} = \mathcal{A}_e \quad \Rightarrow \quad \mathcal{A}_e = -z \frac{\partial C(T, z_e)}{\partial z_e} - \frac{\partial G}{\partial z_e} \frac{z^2}{2} - \frac{z}{2} \left[ \frac{\partial \alpha}{\partial z_e} z + \frac{\partial \beta}{\partial z_e} (1-z) \right] \left( \frac{2}{3} \boldsymbol{\varepsilon}_{\text{tr}} : \boldsymbol{\varepsilon}_{\text{tr}} \right) - \mu \frac{\partial \gamma}{\partial z_e}.$$

Equations (6), (7), (8), and (9) allow us to establish the stress-strain relation

$$\boldsymbol{\sigma} = \mathbf{K} : (\boldsymbol{\varepsilon} - z\boldsymbol{\varepsilon}_{\text{tr}} - \boldsymbol{\varepsilon}_r).$$

$\mathbf{K}$ , the equivalent SMA elastic moduli tensor, is given by

$$\mathbf{K} = [(1-z)\mathbf{K}_A^{-1} + z\mathbf{K}_M^{-1}]^{-1}.$$

**2.2.4. Yield functions and evolution laws.** Residual strain and internal stress depend on the number of loading cycles. Indeed, as shown in Figure 2, left, residual strain is found to increase exponentially with respect to the number of cycles up to an asymptotic value  $\boldsymbol{\varepsilon}_r^{\text{sat}}$ . From a theoretical point of view, this can be simulated using the evolution law

$$\dot{\boldsymbol{\varepsilon}}_r = \frac{\varepsilon_r^{\text{sat}}}{\tau} \left( \frac{3}{2} \frac{\mathbf{s}}{\sigma_{\text{VM}}} \right) \exp\left(-\frac{z_e}{\tau}\right) \dot{z}_e.$$

Residual strain is considered to be deviatoric and so it does not induce any volume change.  $\tau$  is a time constant,  $\varepsilon_r^{\text{sat}}$  is the maximum residual strain in tension when the hysteresis loop stabilizes,  $\mathbf{s}$  is the deviatoric part of the stress tensor, and  $\sigma_{\text{VM}}$  is the equivalent Von Mises measure on the stress tensor. Dissipation due to the evolution of  $\boldsymbol{\varepsilon}_r$  is necessarily positive. Indeed, it can easily be shown that  $\mathcal{A}_r$  is unconditionally equal to the stress tensor  $\boldsymbol{\sigma}$ .  $\mathcal{A}_r : \dot{\boldsymbol{\varepsilon}}_r$  is therefore positive. Similarly, the evolution of internal stress  $\mathbf{B}$  is assumed to be governed by the equation

$$\dot{\mathbf{B}} = \frac{B^{\text{sat}}}{\tau} \left( \frac{2}{3} \boldsymbol{\varepsilon}_{\text{tr}} / \sqrt{\frac{2}{3} \boldsymbol{\varepsilon}_{\text{tr}} : \boldsymbol{\varepsilon}_{\text{tr}}} \right) \exp\left(-\frac{z_e}{\tau}\right) \dot{z}_e, \quad (10)$$

where  $B^{\text{sat}}$  is a positive scalar.

Equation (10) expresses an increase in equivalent internal stress with respect to the number of cycles. Given the expression of the thermodynamic force  $\mathcal{A}_B$  associated with state variable  $\mathbf{B}$ , dissipation  $\mathcal{A}_B : \dot{\mathbf{B}}$  is positive. Because the evolution of state variables  $\boldsymbol{\varepsilon}_r$ ,  $\mathbf{B}$ , and  $z_e$  is related to that of the martensite volume fraction, one does not need to define specific yield functions for each of these variables. Nevertheless, three yield functions:  $\mathcal{F}_z^1$ ,  $\mathcal{F}_z^2$ , and  $\mathcal{F}_{\text{ori}}$  are needed in order to describe forward phase change, reverse phase change, and orientation of martensite variants. Thermodynamic forces  $\mathcal{A}_z$  and  $\mathcal{A}_{\text{tr}}$  are chosen to be such that

$$\mathcal{A}_z \in \partial_{\dot{z}} \mathcal{D}, \quad \mathcal{A}_{\text{tr}} \in \partial_{\dot{\boldsymbol{\varepsilon}}_{\text{tr}}} \mathcal{D}, \quad (11)$$

where  $\mathcal{D}$  is a convex positive continuous function that is equal to zero at the origin:

$$\mathcal{D} \stackrel{\text{def}}{=} D(\dot{z}, \dot{\boldsymbol{\varepsilon}}_{\text{tr}}) = P(z, z_e, \dot{z}) \dot{z} + R(z) \sqrt{\frac{2}{3} \dot{\boldsymbol{\varepsilon}}_{\text{tr}} : \dot{\boldsymbol{\varepsilon}}_{\text{tr}}}, \quad (12)$$

with

$$P(z, z_e, \dot{z}) \stackrel{\text{def}}{=} [a(1-z) + bz] \text{sign } \dot{z},$$

for certain  $z_e$ -dependent parameters  $a = \hat{a}(z_e)$  and  $b = \hat{b}(z_e)$ . Moreover,  $R(z) = z^2 Y$ , where  $Y$  is a constant material parameter. It is easy to show that  $Y$ ,  $a$ , and  $b$  are always positive;  $\mathcal{D}$  is therefore positive. Hence, evolution equations (11) necessarily satisfy the Clausius–Duhem inequality.

From this point on, austenite and martensite are considered to be homogeneous and isotropic media, having the same Poisson coefficient  $\nu$ . Specifically,

$$\nu_A = \nu_M \stackrel{\text{def}}{=} \nu.$$

Table 1 summarizes the notations used throughout this paper. Using equations (11), one can establish

Meaning or Expression		Meaning	Expression
$E_A$	Young modulus of austenite	$E_{eq}$	Equivalent Young modulus $\left(\frac{1-z}{E_A} + \frac{z}{E_M}\right)^{-1}$
$E_M$	Young modulus of martensite	$\text{tr } \mathbf{M}$	Trace of symmetrical tensor $\mathbf{M}$ $\sum_i \mathbf{M}_{ii}$
$\nu$	Poisson coefficient	$\text{dev } \mathbf{M}$	Deviator of $\mathbf{M}$ $\mathbf{M} - \frac{1}{3}(\text{tr } \mathbf{M}) \mathbf{I}$
$El_A$	$(1+\nu)/E_A$	$M_{VM}$	Von Mises equivalent of $\mathbf{M}$ $\sqrt{\frac{3}{2} \text{dev } \mathbf{M} : \text{dev } \mathbf{M}}$
$El_M$	$(1+\nu)/E_M$	$\mathbf{s}$	Stress deviator tensor $\text{dev } \boldsymbol{\sigma}$
$P_A$	$-\nu/E_A$	$\sigma_{VM}$	Von Mises equivalent stress $\sqrt{\frac{3}{2} \mathbf{s} : \mathbf{s}}$
$P_M$	$-\nu/E_M$	$\mu_A$	Austenite shear modulus $\frac{1}{2} E_A / (1+\nu)$
$El_{MA}$	$El_M - El_A$	$\mu_M$	Martensite shear modulus $\frac{1}{2} E_M / (1+\nu)$
$P_{MA}$	$P_M - P_A$	$\mu_{eq}$	Equivalent shear modulus $\frac{1}{2} E_{eq} / (1+\nu)$

**Table 1.** Notations used in this paper.

expressions for  $\mathcal{F}_z^1$ ,  $\mathcal{F}_z^2$ , and  $\mathcal{F}_{ori}$ :

$$\mathcal{F}_z^1 = \left\{ \frac{1}{3} El_{MA} \sigma_{VM}^2 + \frac{1}{2} \left( \frac{1}{3} El_{MA} + P_{MA} \right) (\text{tr } \boldsymbol{\sigma})^2 - C(T, z_e) \right\} + \left( \boldsymbol{\sigma} + \frac{2}{3} \mathbf{B} \right) : \boldsymbol{\epsilon}_{tr} - (G+b)z - a(1-z) - \left[ (\alpha - \beta)z + \frac{1}{2}\beta \right] \left( \frac{2}{3} \boldsymbol{\epsilon}_{tr} : \boldsymbol{\epsilon}_{tr} \right),$$

$$\mathcal{F}_z^2 = - \left\{ \frac{1}{3} El_{MA} \sigma_{VM}^2 + \frac{1}{2} \left( \frac{1}{3} El_{MA} + P_{MA} \right) (\text{tr } \boldsymbol{\sigma})^2 - C(T, z_e) \right\} - \left( \boldsymbol{\sigma} + \frac{2}{3} \mathbf{B} \right) : \boldsymbol{\epsilon}_{tr} + (G-b)z - a(1-z) + \left[ (\alpha - \beta)z + \frac{1}{2}\beta \right] \left( \frac{2}{3} \boldsymbol{\epsilon}_{tr} : \boldsymbol{\epsilon}_{tr} \right),$$

$$\mathcal{F}_{ori} = \left\| \left( \boldsymbol{\sigma} + \frac{2}{3} \mathbf{B} \right) - \frac{2}{3} [\alpha z + \beta(1-z)] \boldsymbol{\epsilon}_{tr} - \frac{2\mu}{3z} \boldsymbol{\epsilon}_{tr} / \sqrt{\frac{2}{3} \boldsymbol{\epsilon}_{tr} : \boldsymbol{\epsilon}_{tr}} \right\|_{VM} - zY.$$

It is worth noting that in each of these expressions, a quantity  $\frac{2}{3} \mathbf{B}$ , proportional to internal stress due to training, is added to the stress tensor  $\boldsymbol{\sigma}$ . Thus both  $\mathbf{B}$  and  $\boldsymbol{\sigma}$  have similar effects on phase change and martensite orientation.

Phase change evolution laws obey certain conditions

- If  $\mathcal{F}_z^1 < 0$  and  $\mathcal{F}_z^2 < 0$ , no phase change can occur. Hence,  $\dot{z} = 0$ .
- If forward phase change is triggered,  $\mathcal{F}_z^1$  is equal to zero. In this case,  $\dot{z}$  is equal to zero if  $\dot{\mathcal{F}}_z^1 < 0$ ; otherwise,  $\dot{z}$  is given by the consistency condition  $\dot{\mathcal{F}}_z^1 = 0$ .
- If reverse phase change is triggered,  $\mathcal{F}_z^2$  is equal to zero. In this case,  $\dot{z}$  is equal to zero if  $\dot{\mathcal{F}}_z^2 < 0$ ; otherwise,  $\dot{z}$  is given by the consistency condition  $\dot{\mathcal{F}}_z^2 = 0$ .

Let

$$\mathbf{X} \stackrel{\text{def}}{=} \left( \mathbf{s} + \frac{2}{3} \mathbf{B} \right) - \frac{2}{3} [\alpha z + \beta(1-z)] \boldsymbol{\epsilon}_{tr} - \frac{2\mu}{3z} \boldsymbol{\epsilon}_{tr} / \sqrt{\frac{2}{3} \boldsymbol{\epsilon}_{tr} : \boldsymbol{\epsilon}_{tr}}.$$

The yield function  $\mathcal{F}_{\text{ori}}$ , associated with martensite orientation, can be written as  $\mathcal{F}_{\text{ori}} = X_{\text{VM}} - zY$ . Evolution of the local inelastic strain tensor  $\boldsymbol{\epsilon}_{\text{tr}}$  satisfies the normality law:

$$\dot{\boldsymbol{\epsilon}}_{\text{tr}} = \eta \frac{\partial \mathcal{F}_{\text{ori}}}{\partial \mathbf{X}} = \frac{3}{2} \eta \frac{\mathbf{X}}{X_{\text{VM}}}. \quad (13)$$

Here  $\eta$  is a positive scalar satisfying the Kuhn–Tucker conditions

$$\eta \geq 0, \quad \mathcal{F}_{\text{ori}} \leq 0 \quad \text{and} \quad \eta \mathcal{F}_{\text{ori}} = 0.$$

Let  $\sigma_{\text{rs}}$  and  $\sigma_{\text{rf}}$  be orientation start and finish stresses of self-accommodating martensite

- When orientation starts, the yield function  $\mathcal{F}_{\text{ori}}$  is necessarily equal to zero for  $\mu = 0$ ,  $\boldsymbol{\epsilon}_{\text{tr}} = \mathbf{0}$ , and  $\|\boldsymbol{\sigma} + \mathbf{B}\|_{\text{VM}} = \sigma_{\text{rs}}$ . It follows that

$$Y = \sigma_{\text{rs}}; \quad (14)$$

- When orientation is complete,  $\mathcal{F}_{\text{ori}} = 0$  for  $\sqrt{\frac{2}{3}} \boldsymbol{\epsilon}_{\text{tr}} : \boldsymbol{\epsilon}_{\text{tr}} = \gamma$ . If  $\sqrt{\frac{2}{3}} \boldsymbol{\epsilon}_{\text{tr}} : \boldsymbol{\epsilon}_{\text{tr}}$  tends towards  $\gamma$  with lower values,  $\mu$  is equal to zero for  $\|\boldsymbol{\sigma} + \mathbf{B}\|_{\text{VM}} = \sigma_{\text{rf}}$ . In case of uniaxial tension, it follows that

$$|\sigma_{\text{rf}} - \alpha \gamma| = Y;$$

the above equation, together with Equation (14), gives  $\alpha$  as a function of  $\gamma$

$$\alpha = \frac{\sigma_{\text{rf}} - \sigma_{\text{rs}}}{\gamma}.$$

- When austenite transforms into oriented martensite, orientation is complete when the stress becomes greater or equal to  $\sigma_{\text{rf}}$ . Particularly, if the stress tends towards  $\sigma_{\text{rf}}$  with lower values,  $\mu$  remains equal to zero. In this case,

$$z = 0, \quad \|\boldsymbol{\sigma} + \mathbf{B}\|_{\text{VM}} = \sigma_{\text{rf}}, \quad \sqrt{\frac{2}{3}} \boldsymbol{\epsilon}_{\text{tr}} : \boldsymbol{\epsilon}_{\text{tr}} = \gamma, \quad \text{and} \quad \mu = 0.$$

In case of uniaxial tension

$$\beta = \frac{\sigma_{\text{rf}}}{\gamma}.$$

$\alpha$  and  $\beta$  are both functions of  $z_e$  due to their dependence on  $\gamma$ . Finally, explicit expressions of the evolution laws can be derived using the consistency conditions.

**2.3. Numerical simulation.** Figure 3, left shows the experimental response of a NiTi test sample to repeated uniaxial tension. Residual strain evolution with respect to the number of cycles is shown in Figure 3, right. The nickel-titanium used in the experiments has an orientation start stress of 80 MPa and an orientation finish stress equal to 160 MPa. The reverse transformation finish temperature of the untrained material at zero stress is equal to 42°C; this temperature does not evolve considerably with the number of cycles. Figure 4 shows good agreement between experimental and numerical results in the case of repeated tension. For clarity, only loops 2, 4, and 12 are shown. Figure 5 (left) illustrates the evolution of internal strain  $B$  with respect to the cumulated martensite volume fraction  $z_e$ . Stress-strain response for all 20 loading cycles is shown in Figure 5 (right).

The next section is devoted to the presentation of an energy approach to the fatigue of shape memory alloys. It is shown how the cyclic model presented in the previous section can be combined with the

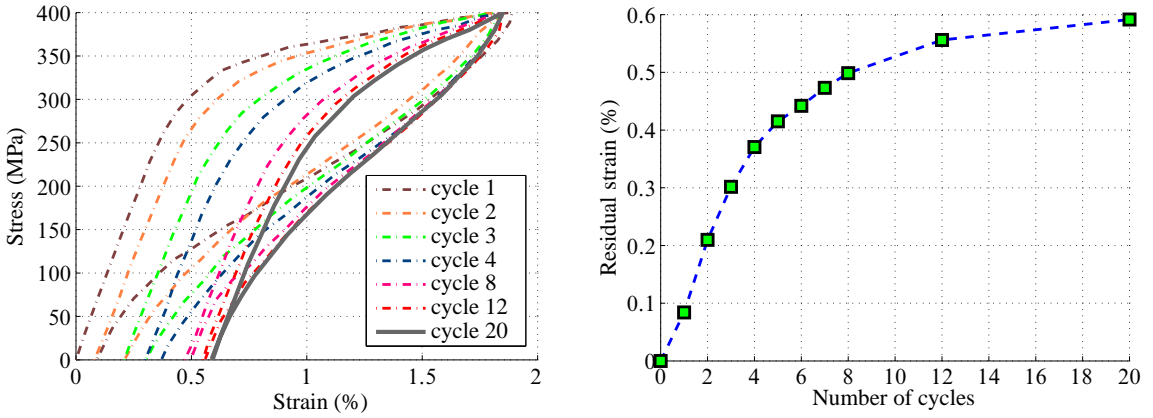


**Figure 3.** Left: experimental stress-strain response of a NiTi wire to repeated tension. The stabilized cycle is shown by a continuous line. Right: residual strain evolution with respect to the number of tension cycles.

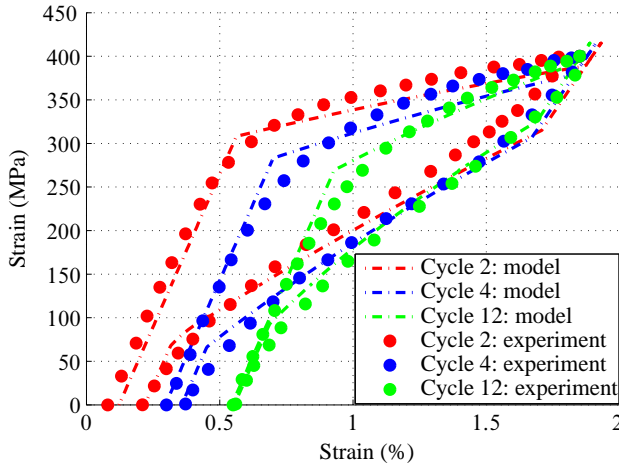


**Figure 4.** Experimental versus numerical results: evolution of the superelastic loop.

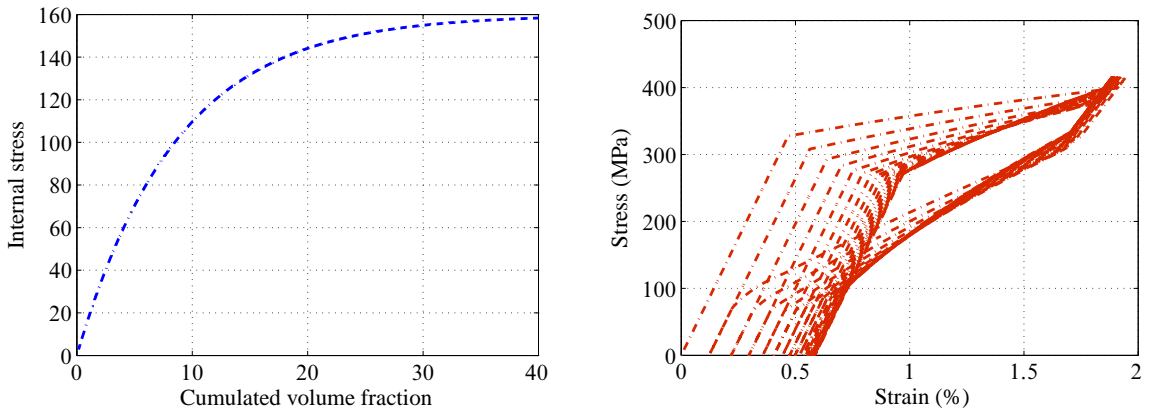


**Figure 5.** Prediction of nickel-titanium response to repeated tension with the evolution of internal stress (left) and the stress-strain response cycles (right).

fatigue criterion in order to perform numerical calculations of the fatigue parameters necessary for the evaluation of the life time of structures made on SMAs.

### 3. An energy approach to the fatigue of shape memory alloys

Fatigue of shape memory alloys is generally explained by the creation and propagation of defects within the material at the microscopic level [Melton and Mercier 1979a]. A more rigorous understanding is complicated, however, due to phenomena like formation of residual martensite [Siredey et al. 2005] and local phase changes at the tip of microscopic cracks [Wagner et al. 2004] resulting in slower crack propagation in martensite [Eggeler et al. 2004]. Because of similar damage creation and propagation mechanisms, it is interesting to investigate the fatigue of SMAs within a framework similar to that of usual elastoplastic materials (like steel). It is, hence, useful to distinguish between low-cycle fatigue, finite fatigue life in high-cycle fatigue, and high-cycle fatigue (infinite life). We will focus on low-cycle fatigue associated with cyclic superelasticity.

#### 3.1. Experimental analysis.

**3.1.1. Material and thermomechanical treatment.** The material is a 51.3% Ti–48.7% Ni in mass nickel-titanium with a grain size between  $60\ \mu\text{m}$  and  $70\ \mu\text{m}$  (see Figure 6). The phase change temperatures at zero stress are as follows  $M_f^0 = 25^\circ\text{C}$ ,  $M_s^0 = 39^\circ\text{C}$ ,  $A_s^0 = 29^\circ\text{C}$  and  $A_f^0 = 42^\circ\text{C}$ . All the test specimens

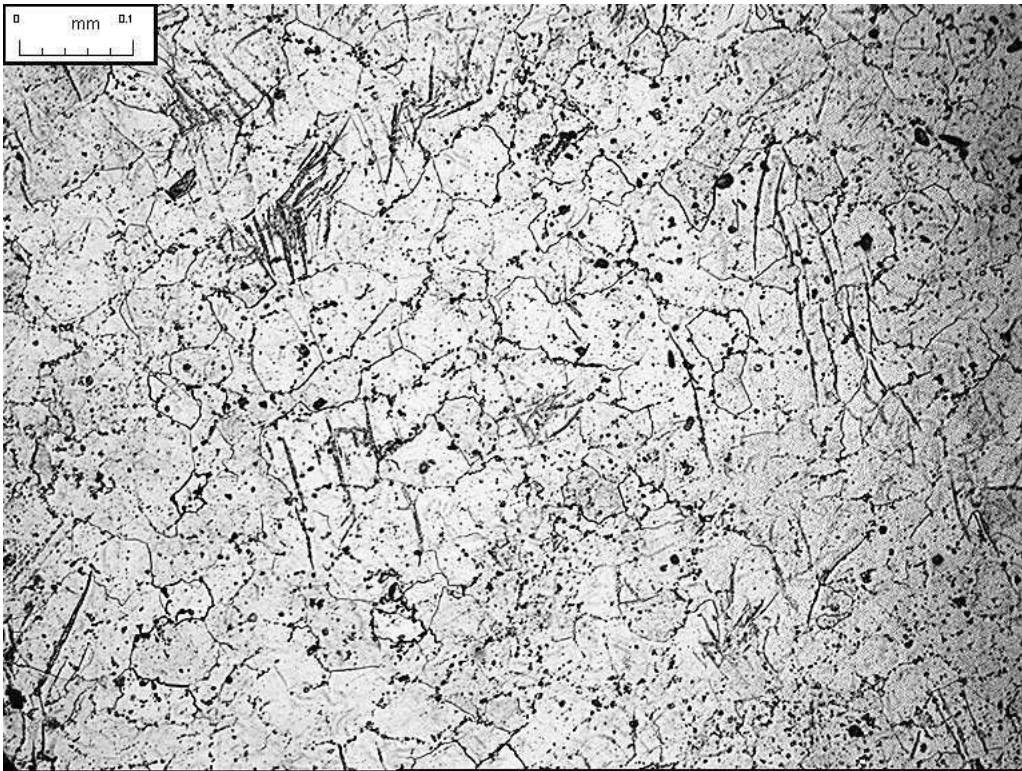


**Figure 6.** Metallographic structure of the NiTi alloy.

were worked up to 20% in tension while cold, then heat treated at 400°C for one hour. This kind of treatment increases the plastic yield limit of the material while improving its superelasticity [Wayman and Otsuka 1999].

**3.1.2. Experimental setup.** The testing machine used is a force controlled MTS810/100KN. The strains are measured using an MTS extensometer model 632-13C-21. Load and extensometer signals are captured by an MTS TestStarII data acquisition board and processed by a computer. Experiments are Stress-controlled push-pull tests with a constant amplitude  $\sigma_a$ . They are carried out at a frequency of 0.3 Hz. In order to ensure that the tests are performed in the pseudoelastic domain the temperature is kept constant at  $T = 50^\circ\text{C}$  which is higher than the austenite finish temperature  $A_f^0$ . The experiments were conducted in a SERVATHIN hermetic enclosure where the temperature can be regulated and kept constant through a range values from  $-50^\circ\text{C}$  to  $200^\circ\text{C}$ . Maximum stress was kept below the critical stress for slip (750 MPa) to ensure that no macroscopic plastic deformations occurs. The tests were taken through to rupture of the specimen.

In order to examine the effect of mean stress on the fatigue of nickel-titanium, three load ratios ( $R = \sigma_{\min}/\sigma_{\max}$ ) were considered, equal to 0, 0.2, and  $-1$  respectively. The geometry of the specimens we used is illustrated in Figure 7.

**3.2. Results and discussions.**

**3.2.1. S-N curves.** The S-N curves (Wöhler curves) relating the number of cycles to failure under uniaxial loading to the amplitude of the applied stress obtained for these experiments are shown on Figure 8. The effect of mean stress on fatigue life can be observed. Indeed, a higher mean stress corresponds to a lower number of cycles to failure. These Wöhler curves can be used for fatigue life prediction when the applied loading is uniaxial and for a given mean stress. They are inadequate, however, for fatigue analysis of shape memory structures under multiaxial loading.

**3.2.2. Low-cycle fatigue life prediction for superelastic SMAs.** Existing SMA low-cycle fatigue life prediction models are mostly of the Manson-Coffin type where the number of cycles to failure is related to the amplitude of plastic strain. As early as 1979, [Melton and Mercier 1979a] showed that, for different types of shape memory alloys, fatigue life of wires follows the Manson-Coffin law. This result has been confirmed in several subsequent papers [Tolomeo et al. 2000; Wagner et al. 2004]. Even though multiaxial loading can be accounted for theoretically by means of a generalized Manson-Coffin relationship using

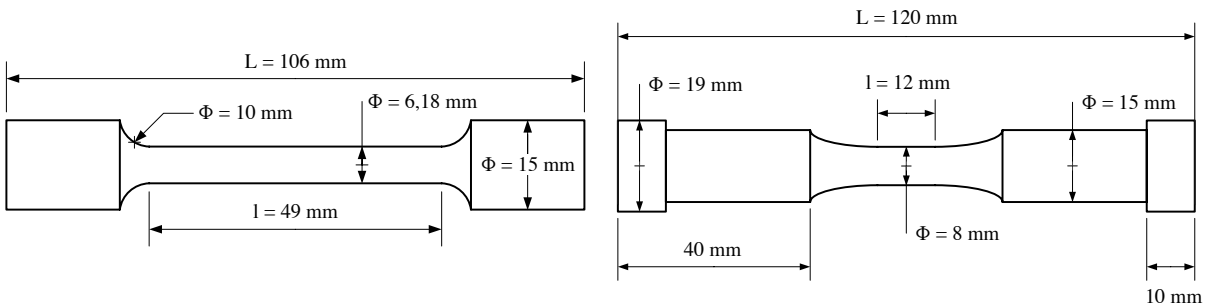


**Figure 7.** Geometries of specimens used for cyclic experiments for  $R = 0$  (left) and  $R = 0.2, -1$  (right), respectively.

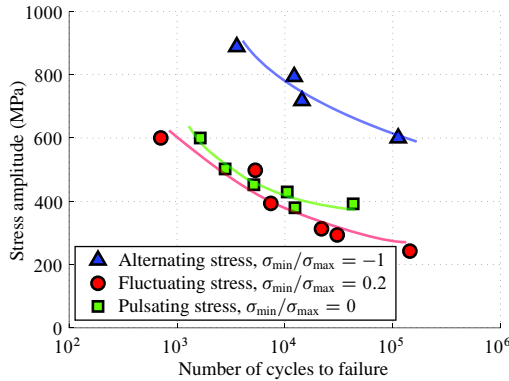


**Figure 8.** Wöhler curves of nickel-titanium for different mean stress values.

equivalent plastic strain, the ability to predict three-dimensional structure failure using this approach has not been proved.

In the scope of this paper, an energy-based approach is used for estimating low-cycle fatigue life of superelastic SMAs. This is inspired from Charkaluk et al. [2002], where a similar approach was successfully applied on cast iron. Indeed, superelastic hysteresis stabilization for a shape memory material is similar to plastic shakedown of cast iron. In both cases, inelastic (plastic deformation for iron cast and transformation strain for SMAs) deformation is confined but the material continues to dissipate energy. Energy dissipation is usually explained, in the case of superelastic SMAs, by strain incompatibilities across the boundaries of the grains [Melton and Mercier 1979b] which in time lead to the creation and accumulation of defects at the boundaries [Melton and Mercier 1979a].

In this paper, the martensitic transformation, responsible for the creation of martensite grains, is accounted for using state variables  $z$  and  $\varepsilon_{tr}$ . Given the above interpretation of energy dissipation in SMAs, the inelastic deformation  $z\varepsilon_{tr}$ , being proportional to the number of martensite grain boundaries (through state variable  $z$ ) and to the level of orientation of martensite variants within these grains, seems an adequate parameter for predicting fatigue failure of superelastic SMAs.

The amount of dissipated energy per loading cycle,  ${}^{\circ}W_d$ , is given by

$${}^{\circ}W_d = \oint \boldsymbol{\sigma} : d\boldsymbol{\varepsilon}.$$

Once the material response stabilizes, this energy becomes constant, as shown by the experimental result given in Figure 9, left (stress ratio = 0).

In the case of the studied nickel-titanium, an example of the evolution of the dissipated energy with respect to the number of cycles is illustrated in Figure 9, right. Even though the use of dissipated energy per cycle for fatigue life prediction has been criticized [Halford 1966; Pineau and Pétrequin 1997], its usefulness in practice is well proven. The work of [Charkaluk et al. 2002] has been successfully applied to predicting failure of automotive components subjected to complex thermomechanical loading.

The data points in Figure 10, left, represent the amount of dissipated energy per cycle  ${}^{\circ}W_d$  with respect to the number of cycles to failure  $N_f$ , plotted on a log-log scale. The figure shows a quasilinear dependence of  $\log {}^{\circ}W_d$  on  $\log N_f$  for several values of the mean stress. Hence it is interesting to approximate

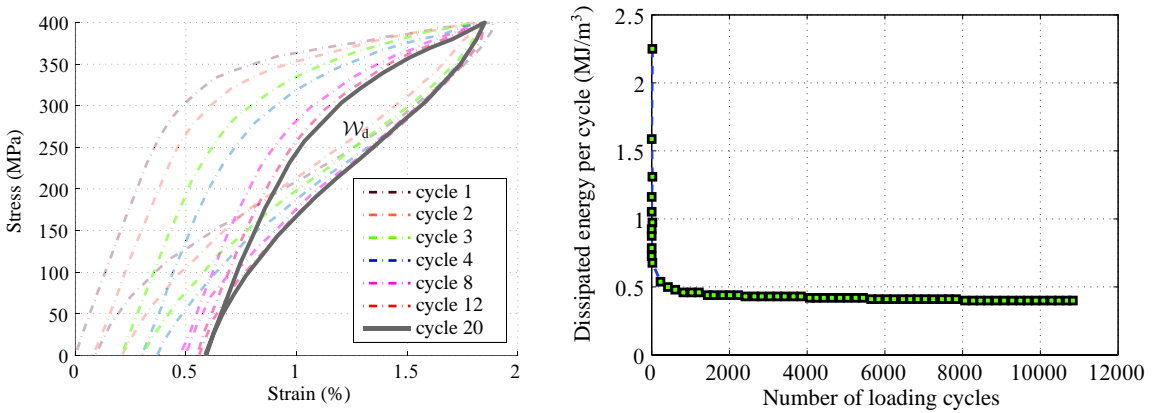


**Figure 9.** Left: experimental stabilization of the amount of dissipated energy per cycle,  $W_d$ , with the number of cycles. Right: dissipated energy per cycle versus number of loading cycles: experimental result for  $\Delta\sigma = 400\text{Mpa}$ .

the experimental results using the following curve from [Moumni et al. 2005]:

$$W_d = \alpha N_f^\beta, \tag{15}$$

where  $\alpha$  and  $\beta$  are material parameters. This is shown as the gray line in the same figure. Expression (15) can readily be used for three-dimensional structure analysis because dissipated energy per cycle is well defined and its calculation is straightforward.

The stabilized cycle and the corresponding amount dissipated energy to the stabilized cycle can be numerically determined using the model presented in this paper as shown in Figure 10, right. The number of cycles to failure of a SMA structure can be estimated using the suggested fatigue criterion.

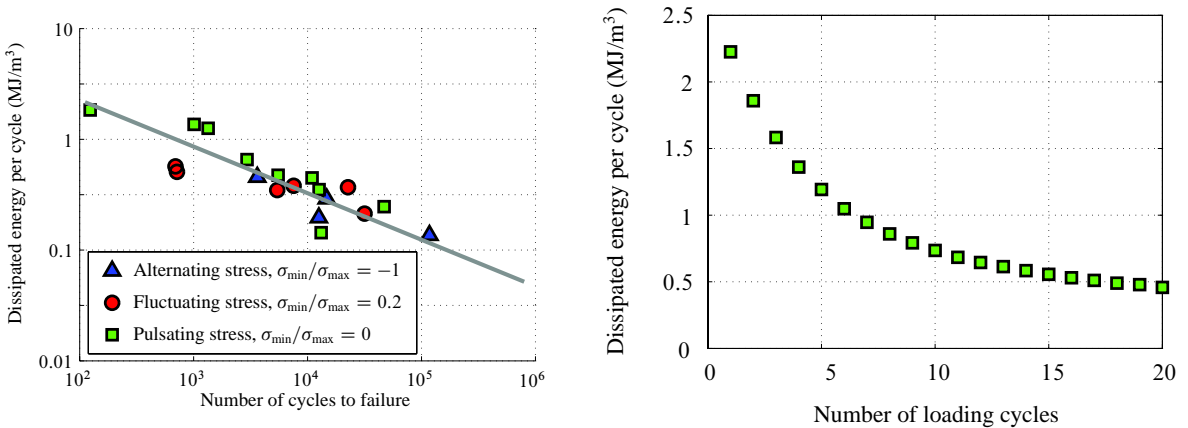


**Figure 10.** Left: experimental results for dissipated energy per cycle as a function of the number of cycles to failure, for  $\alpha = 11$  and  $\beta = -0.377$ , and fit using Equation (15). Right: numerical results for dissipated energy per cycle with respect to the number of cycles, with  $\Delta\sigma = 400\text{Mpa}$ .

It is important to note, however, that the validity of this criterion has only been proven in the case of uniaxial loading; its ability to predict failure of structures subjected to complicated loading conditions remains to be established.

#### 4. Conclusion

In the first part of this paper, a model capable of simulating several phenomena associated with shape memory materials subjected to cyclic loading is presented. The modeling process is based on a simple observation. On the macroscopic level, SMA training can be interpreted as a thermomechanically-induced transition from an unstable virgin material configuration into a stable one. From a theoretical point of view, it is easy to account for this transition by making some of the model parameters depend on a cumulated martensite volume fraction which evolves with the applied loading. Inelastic residual strain, which appear during repeated phase change, is accounted for by introducing a state variable similar to plastic deformation strain of classical elastoplastic materials. Numerical results show good agreement with available experimental data.

The second part of the paper investigates the fatigue of SMAs by analogy with plastic fatigue. It has been shown that the dissipated energy at the stabilized cycle during a cyclic loading is a relevant parameter for fatigue life prediction. A relationship between this parameter and the number of cycles to failure has been derived from experimental results. It has also been shown that the cyclic model can be combined with the fatigue criterion in order to predict low-cycle failure of superelastic shape memory structures. Nevertheless, it is clear that the model must be improved on some points. First, it is important to investigate the fatigue of SMAs criterion for another type of loading, namely torsion. Second, it is interesting to check the validity of the model against experimental results for complex structures under complex loading. This work is undertaken and will be presented in future papers.

#### References

- [Abeyaratne and Kim 1997] R. Abeyaratne and S.-J. Kim, "Cyclic effects in shape-memory alloys: a one-dimensional continuum model", *Int. J. Solids Struct.* **34**:25 (1997), 3273–3289.
- [Auricchio et al. 2003] F. Auricchio, S. Marfia, and E. Sacco, "Modelling of SMA materials: training and two way memory effects", *Comput. Struct.* **81**:24-25 (2003), 2301–2317.
- [Bo and Lagoudas 1999] Z. Bo and D. C. Lagoudas, "Thermomechanical modeling of polycrystalline SMAs under cyclic loading, I: theoretical derivations", *Int. J. Eng. Sci.* **37**:9 (1999), 1089–1140.
- [Charkaluk et al. 2002] E. Charkaluk, A. Bignonnet, A. Constantinescu, and K. D. Van, "Fatigue design of structures under thermomechanical loadings", *Fatigue Fract. Eng. Mater. Struct.* **25**:12 (2002), 1199–1206.
- [Eggeler et al. 2004] G. Eggeler, E. Hornbogen, A. Yawny, A. Heckmann, and M. Wagner, "Structural and functional fatigue of NiTi shape memory alloys", *Mater. Sci. Eng. A* **378**:1-2 (2004), 24–33.
- [Halford 1966] G. Halford, "The energy required for fatigue", *J. Mater.* **1** (1966), 3–18.
- [Leclerq and Lexcellent 1996] S. Leclerq and C. Lexcellent, "A general macroscopic description of the thermomechanical behavior of shape memory alloys", *J. Mech. Phys. Solids* **44**:6 (1996), 953–957.
- [Lexcellent and Bourbon 1996] C. Lexcellent and G. Bourbon, "Thermodynamical model of cyclic behaviour of ti-ni and cu-zn-al shape memory alloys under isothermal undulated tensile tests", *Mech. Mater.* **24**:1 (1996), 59–73.
- [Lim and McDowell 2002] T. J. Lim and D. L. McDowell, "Cyclic thermomechanical behavior of a polycrystalline pseudoelastic shape memory alloy", *J. Mech. Phys. Solids* **50**:3 (2002), 651–676.

- [Liu et al. 1999] Y. Liu, Z. Xie, and J. Van Humbeeck, "Cyclic deformation of NiTi shape memory alloys", *Mater. Sci. Eng. A* **273–275** (1999), 673–678.
- [McKelvey and Ritchie 1999] A. L. McKelvey and R. O. Ritchie, "Fatigue-crack propagation in Nitinol, a shape-memory and superelastic endovascular stent material", *J. Biomed. Mater. Res.* **47:3** (1999), 301–308.
- [Melton and Mercier 1979a] K. N. Melton and O. Mercier, "The effect of the martensitic phase transformation on the low cycle fatigue behaviour of polycrystalline Ni–Ti and Cu–Zn–Al alloys", *Mat. Sci. Eng.* **40:1** (1979), 81–87.
- [Melton and Mercier 1979b] K. N. Melton and O. Mercier, "Fatigue life of cuznal alloys", *Scr. Metall. Mater.* **13:1** (1979), 73–75.
- [Melton and Mercier 1979c] K. N. Melton and O. Mercier, "Fatigue of NiTi thermoelastic martensites", *Acta Metall.* **27:1** (1979), 137–144.
- [Miyazaki et al. 1986] S. Miyazaki, T. Imai, Y. Igo, and K. Otsuka, "Effect of cyclic deformation on the pseudoelasticity characteristics of Ti-Ni alloys", *Metall. Mater. Trans. A* **17:1** (1986), 115–120.
- [Morgan 2004] N. B. Morgan, "Medical shape memory alloy applications—the market and its products", *Mater. Sci. Eng. A* **378:1-2** (2004), 16–23.
- [Moumni et al. 2005] Z. Moumni, A. V. Herpen, and P. Riberty, "Fatigue analysis of shape memory alloys: energy approach", *Smart Mater. Struct.* **14:5** (2005), S287–S292.
- [Moumni et al. 2008] Z. Moumni, W. Zaki, and Q. S. Nguyen, "Theoretical and numerical modeling of solid-solid phase change: application to the description of the thermomechanical behavior of shape memory alloys", *Int. J. Plast.* **24:4** (2008), 614–645.
- [Patoor and Berveiller 1993] E. Patoor and M. Berveiller, "Lois de comportement et calcul de structures en alliage à mémoire de forme", Chapter 9, pp. 195–224 in *Technologie des alliages à mémoire de forme*, Hermes, Paris, 1993.
- [Pineau and Pétrequin 1997] A. Pineau and P. Pétrequin, *La fatigue des matériaux et des structures*, 2<sup>e</sup> ed., Chapter 4, pp. 155–214, Hermes, Paris, 1997.
- [Porter et al. 2001] G. A. Porter, P. K. Liaw, T. N. Tieg, and K. H. Wu, "Fatigue and fracture behavior of nickel-titanium shape-memory alloy reinforced aluminum composites", *Mater. Sci. Eng. A* **314:1-2** (2001), 186–193.
- [Predki et al. 2006] W. Predki, M. Klönne, and A. Knopik, "Cyclic torsional loading of pseudoelastic NiTi shape memory alloys: damping and fatigue failure", *Mater. Sci. Eng. A* **417:1-2** (2006), 182–189.
- [Raniecki et al. 1992] B. Raniecki, C. LExcellent, and K. Tanaka, "Thermodynamic models of pseudoelastic behaviour of shape memory alloys", *Arch. Mech.* **44** (1992), 261–284.
- [Shaw and Kyriakides 1995] J. A. Shaw and S. Kyriakides, "Thermomechanical aspects of NiTi", *J. Mech. Phys. Solids* **43:8** (1995), 1243–1281.
- [Siredey et al. 2005] N. Siredey, A. Hautcoeur, and A. Eberhardt, "Lifetime of superelastic Cu–Al–Be single crystal wires under bending fatigue", *Mater. Sci. Eng. A* **396:1-2** (2005), 296–301.
- [Tanaka et al. 1995] K. Tanaka, F. Nishimura, T. Hayashi, H. Tobushi, and C. LExcellent, "Phenomenological analysis on subloops and cyclic behavior in shape memory alloys under mechanical and/or thermal loads", *Mech. Mater.* **19:4** (1995), 281–292.
- [Tolomeo et al. 2000] D. Tolomeo, S. Davidson, and M. Santinoranont, "Cyclic properties of superelastic Nitinol: design implications", pp. 471–476 in *SMST-2000: Proceedings of the International Conference on Shape Memory and Superelastic Technologies* (Pacific Grove, CA), edited by S. M. Russell and A. R. Pelton, International Organization on SMST, 2000.
- [Vaidyanathan et al. 2000] R. Vaidyanathan, D. C. Dunand, and U. Ramamurty, "Fatigue crack-growth in shape-memory Ni-Ti and NiTi-TiC composites", *Mater. Sci. Eng. A* **289:1-2** (2000), 208–216.
- [Van Humbeeck 1991] J. Van Humbeeck, "Cycling effects, fatigue and degradation of shape memory alloys", *J. Phys. (France) IV* **1:C4** (1991), 189–197.
- [Wagner et al. 2004] M. Wagner, T. Sawaguchi, G. Kausträter, D. Höffken, and G. Eggeler, "Structural fatigue of pseudoelastic NiTi shape memory wires", *Mater. Sci. Eng. A* **378:1-2** (2004), 105–109.
- [Wayman and Otsuka 1999] C. M. Wayman and K. Otsuka (editors), *Shape memory alloys*, Cambridge University Press, Cambridge, 1999.

[Zaki 2006] W. Zaki, *Comportement thermo-mécanique des matériaux à mémoire e forme*, Ph.D. thesis, École Polytechnique, 2006, Available at <http://www.imprimerie.polytechnique.fr/Theses/Files/Zaki.pdf>.

[Zaki and Moumni 2007a] W. Zaki and Z. Moumni, “A 3d model of the cyclic thermomechanical behavior of shape memory alloys”, *J. Mech. Phys. Solids* **55**:11 (2007), 2427–2454.

[Zaki and Moumni 2007b] W. Zaki and Z. Moumni, “A three-dimensional model of the thermomechanical behavior of shape memory alloys”, *J. Mech. Phys. Solids* **55**:11 (2007), 2455–2490.

Received 14 Dec 2007. Revised 14 Apr 2008. Accepted 6 Apr 2008.

ZIAD MOUMNI: [moumni@ensta.fr](mailto:moumni@ensta.fr)

UME-MS, École Nationale Supérieure de Techniques Avancées, 91761 Palaiseau Cedex, France

Wael Zaki: [wael.zaki@tudor.lu](mailto:wael.zaki@tudor.lu)

Laboratory for Industrial Technology, Henri Tudor Public Research Center, 66 rue de Luxembourg, L-4221 Esch-sur-Alzette, Luxembourg

HABIBOU MAITOURNAM: [habibou@lms.polytechnique.fr](mailto:habibou@lms.polytechnique.fr)

Laboratoire de Mécanique des Solides, UMR 7649, École Polytechnique, 91128 Palaiseau Cedex, France

